



K-FLEX: A flexible robotic platform for scar-free endoscopic surgery

Minho Hwang | Dong-Soo Kwon

Department of Mechanical Engineering, Korea Advanced Institute of Science and Technology (KAIST), Daejeon, Republic of Korea

Correspondence

Dong-Soo Kwon, Department of Mechanical Engineering, Korea Advanced Institute of Science and Technology (KAIST), 291, Daehak-ro, Yuseong-gu, Daejeon 34141, Republic of Korea.
 Email: kwonds@kaist.ac.kr

Funding information

Korea Advanced Institute of Science and Technology; Ministry of Education, Grant/Award Number: 2008-0060621

Abstract

Background: Despite its high lesion accessibility and versatility, endoscopic platforms have suffered from designing flexible manipulators with high payload capability sufficient to perform advanced endoscopic procedures.

Methods: A flexible robotic platform, K-FLEX, has been developed with a design of 17 mm in overall diameter. To overcome the shape distortion and deflection in payload handling, a strong continuum manipulator has been designed to have maximum resistance to the distortion. The kinematic analysis and mapping strategy have been established for the master-slave teleoperation.

Results: The proposed manipulator has shown 7.5 mm in trajectory variation to lift the weight of 300 g. Finally, the feasibility of the integrated K-FLEX system has been verified through three kinds of simulated surgical tasks.

Conclusions: The initial prototype of the proposed robot showed the possibility of advanced endoscopic surgery with improved payload capability.

KEY WORDS

computer-assisted surgery, continuum robots, flexible manipulator, kinematics mapping, master device, minimally invasive surgery (MIS), surgical robots

1 | INTRODUCTION

Robotic technology has facilitated minimally invasive surgery (MIS) by overcoming the kinematic constraints arising from smaller external incisions. Compared with conventional laparoscopic instruments, robotic instruments have tiny articulated joints at the distal end, which enable the dexterous movement of the end effector. Although robotic MIS is being performed extensively with these advantages, current robotic surgery focuses primarily on the surgical site through the abdominal wall, which allows direct access to the target lesion.

The flexible surgical robot is an emerging platform that is expected to overcome the limitations of rigid surgical robots. Since it can access the target surgical site through a curved path, the flexible robot has the potential to expand its application into various areas of surgery. One promising candidate is gastrointestinal surgery, which requires miniaturization to pass through natural orifices, flexibility to reach the target lesion, and dexterity to perform surgical tasks. Currently, various advanced techniques are being developed in the field

of gastrointestinal surgery using flexible endoscopes. The progress of such techniques, however, has been hindered by the limitations of the conventional endoscope, which specializes in the diagnosis of lumen.

The standard endoscope is not suitable for performing more advanced tasks such as tissue manipulation, traction, and suturing. More technically, the difficulties involve the lack of dexterity of the surgical tip, maintaining spatial orientation, and multitasking control. In particular, the bimanual manipulation of the surgical tip independent from the camera view is a necessary requirement that is hard to be overcome by practical experience of using an existing endoscope.

To overcome these limitations, several endoscopic platforms have been developed for advanced endoluminal procedures. Most of the platforms have a common configuration consisting of an endoscopic camera attached to the actively steerable overtube and the two surgical arms branched from the distal end—EndoSAMURAI,¹ DDES,² and Cobra.³ Although these platforms have increased the efficiency of the procedures with the dexterous end effectors, their manual mode of control requires considerable manpower to control the multiple



components at once, which introduces inefficiency due to interpersonal communication and thus degrades the fine and systematic movement of the endoscope.

Robotic technologies have overcome the limitations of these manual platforms facilitating intuitive and efficient multitasking control on the surgeon's side as well as the precise and intelligent movement of the robot on the patient's side. STRAS,⁴ MASTER,⁵ ViaCath,⁶ FLEX,⁷ i2Snake,⁸ and CYCLOPS⁹ systems have shown the possibility of advanced endoscopic surgery with their highly dexterous robotic arm. However, they also seem to have common difficulties in designing flexible manipulators with sufficient miniaturization and payload capability to perform various intraluminal surgical operations. In addition, the surgical tip should be replaceable to utilize various functions during the surgical operation.

In this paper, we propose an endoscopic platform, K-FLEX, applicable to advanced endoluminal surgery. The proposed robot has a design of 17 mm in overall diameter, which permits access to the gastrointestinal tract. The overtube is capable of handling the weight of 300 g, and the modularized surgical instruments can be easily replaced during surgical procedures, providing various functions.

The main contribution of this study is a design of a flexible endoscopic platform as well as a flexible continuum manipulator with enhanced payload capability. The guidelines and trial and errors provided in this paper might be helpful for researchers in this field to build a flexible endoscopic platform. This paper presents the overall process of developing and validating the initial prototype of K-FLEX. Section 2 describes the main considerations for performing endoluminal surgery, the design process of the strong continuum manipulator, and the kinematic analysis of the system. Sections 3 and 4 mainly describe the verification process of the developed platform through simulated surgical tasks and share the lessons learned from trial and error in the overall development process.

2 | MATERIALS AND METHODS

2.1 | Design considerations of K-FLEX

Conceptual design of the flexible robot system, K-FLEX, has been established, consisting of a surgical instrument module, overtube, driving robot arm, and master console (Figure 1). Specifications of the K-FLEX were determined on the basis of the reference of the existing literatures and a preliminary test. The main design considerations include degrees of freedom (DoFs), joint configurations, overall diameter, and payload capability. The determined design requirements were then finally confirmed by an expert group of surgeons and endoscopists.

Actively controlled DoFs and their joint configurations strongly influence the performance of slave manipulators including design complexity, mechanism construction, and thus dimensional constraints and payload capability. Without exception, all platforms commonly have the same configurations of overtube, including the standard endoscope, which has translational and rotational movement around the central axis of the main stem followed by a bending segment (from proximal to distal direction).¹⁰ The overtube of the K-FLEX follows the same configuration with them. In contrast, the existing platforms have shown large differences in constructing joint configuration of a bimanual surgical arm. A categorization and a structural comparison of the existing multibranched platforms were conducted through a literature review.¹¹ In this study, we chose prospective candidates for flexible endoscopic surgery among the wide diversity of the existing configurations and classified them into two groups on the basis of their configurations of the bimanual arm.

Type A features an armless overtube with jointed tools, which has a similar configuration to the standard dual channel endoscope but differs in that the surgical tool includes a bending section of a

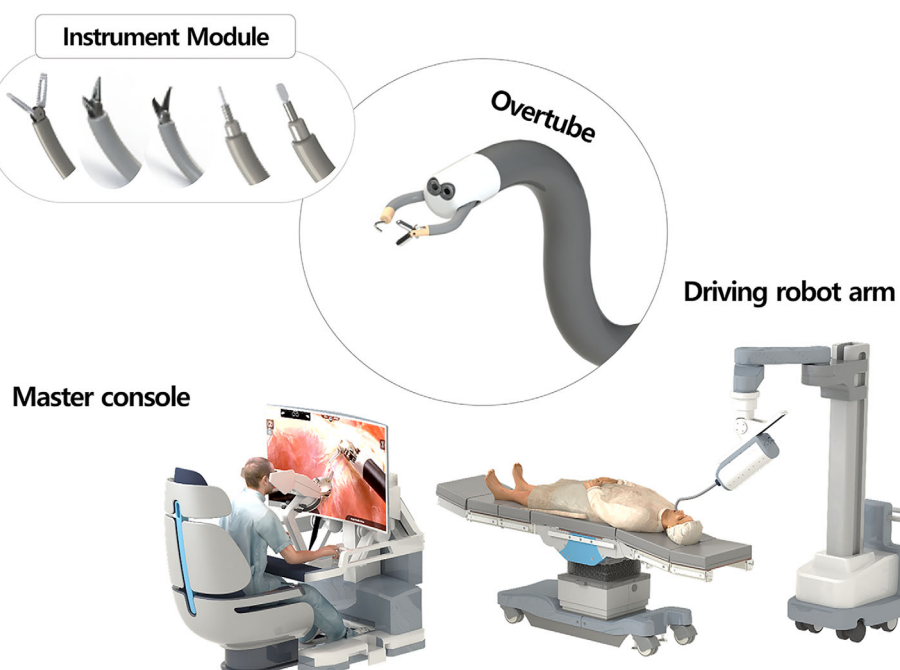


FIGURE 1 The conceptual design of the K-FLEX system, which is composed of surgical instruments, overtube, driving robot arm, and master console



surgical tip. Examples of type A are DDES,² STRAS,⁴ ViaCath,⁶ and FLEX.⁷ They commonly have a translational and rolling segment followed by a deflecting segment at the tip. Since the deflecting segment is close to the tip, small and precise adjustment can be achieved by deflection of the tip after translational and rolling motion of the branch. Following this configuration is also advantageous with regard to clinical practice, facilitating maintenance and sterilization owing to the modularization of the surgical instrument. On the other side, some platforms have followed a configuration, called type B, featuring an armed overtube with jointless tools. In this configuration, the actively steerable branches are fixed at the distal end of the overtube. The identified examples include MASTER⁵ and i2Snake.⁸ Some platforms including EndoSAMURAI,¹ Cobra,³ and CYCLOPS⁹ provide an internal channel inside each steerable branch to allow for exchange of standard surgical instruments. The internal channel also enables the surgical tip to move forward from the steerable branches, creating a large workspace to grasp tissue. Another advantage over type A is a large space for constructing a steering mechanism, which possibly achieves the better performance of the steering. However, the protruding branches can be a dangerous obstacle during insertion through a gastrointestinal pathway. Therefore, an extra guide-tube is necessary for insertion, which results in increasing the overall diameter of the platform. The K-FLEX follows a configuration of type A in consideration of precise manipulation, clinical use, and versatility of the platform. Although type A has a design difficulty in miniaturizing an instrument, the disadvantage will be compensated for by various modularized instruments specialized for each surgical task.

Overall diameter should mainly be considered as an important design criterion for insertion through a natural orifice. To the best of the authors' knowledge, no clear evidence or guidelines exist for the acceptable dimensions of such devices. Referring to the existing

platforms, the diameter varies within a range of 16 to 22 mm for transgastric application.¹⁰ In this study, we defined the design goal of 17 mm for the overall diameter.

Achieving sufficient payload or strength is important for the efficiency of the surgical procedures, but these requirements are difficult to attain for flexible endoscopic platforms because the reduced size of the instrument inflicts an exponential loss to the payload capability. The amount of force required for endoscopic procedures greatly varies depending on the type of procedure.

In this study, a brief preliminary test was performed to approximately estimate the traction force of organs. A partial weight of the ex vivo porcine organs was measured including intestine, stomach, and liver. Each of the organs was hanged with its edge fixed to a force gauge. Following the surgeon's instructions, the organ was partially lifted at the height of 100 mm, which is sufficient for organs to be exposed and resected during a surgical operation, and the corresponding lifting force was recorded (Figure 2). As a result of averaging three specimens, the approximated partial traction weight was measured as 96 g for the small intestine, 57 g for the large intestine, 176 g for the stomach, and 253 g for the liver (Table 1). On the basis of the results, the payload requirement of the manipulator was set to be 300 g. The final design specifications of K-FLEX are summarized in Table 2.

2.2 | Design of a strong continuum manipulator

The continuum manipulator is essential in flexible robots. In order to be inserted into a flexible pathway, a bending section should be consisted of a number of consecutive links, which results in underactuated or redundant characteristics of the manipulator. This

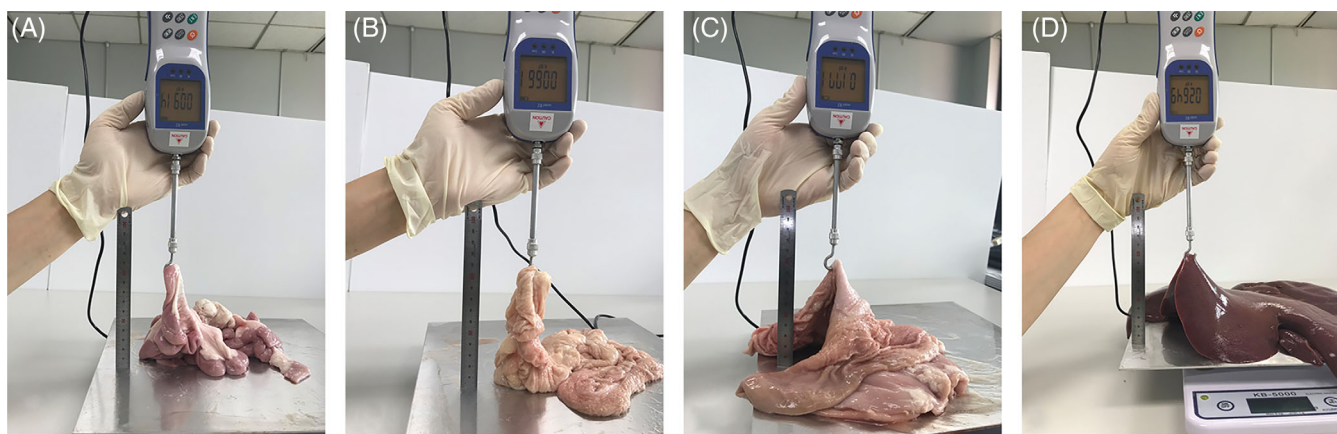


FIGURE 2 To approximate a traction force, a partial weight of an ex vivo organ was measured. Each organ was partially lifted with its edge hanged to a force gauge, and the corresponding lifting force was recorded: (A) small intestine, (B) large intestine, (C) stomach, and (D) liver

TABLE 1 Approximate total and partial weight of ex-vivo organs

	Small Intestine	Large Intestine	Stomach	Liver
Total weight, g	433	321	597	1893
Partial weight, g	96	57	176	253



leads to the common problem of shape distortion in payload handling. Standard endoscopes have a significant amount of shape distortion and deflection as well (Figure 3).

Various methods have been attempted to secure the required stiffness of flexible continuum using shape-memory materials, granular/layer jamming, rheological fluids, and mechanical solutions. However, the previous studies still have limitations in endoscopic applications in terms of external diameter (<15 mm), stiffness (0.9–3.3 N), device temperature (<41°C), and biocompatibility.¹² The spatial constraint in this study is even stricter to include two surgical instruments and an endoscopic camera. Consequently, the bending structure of the overtube should be simple enough to be implemented within a cylindrical thickness of 2 mm to satisfy the overall diameter of 17 mm.

In this study, we utilize the design of a rolling joint to overcome the problem. Although rolling contact joints have been widely employed in continuum robots, they mainly focus on the miniaturized design and their bending behavior without external interactions.¹³ In order to support the sufficient forces for surgical operations, the analysis and design guidelines are required in consideration of the payload handling context. More specifically, the shape of the link will be designed so that the accumulated energy level is minimized when the continuum has a constant curvature rather than a distorted one. Figure 4 shows the concept of the basic rolling joint moving in contact with the rolling surfaces.

The main design variables that determine the characteristics of the continuum manipulator are the rolling radius R , the height of the wire hole B , and the distance between the central axis and the wire hole d . From a geometric relationship, the length of the driving wire cable of a single joint is calculated as follows.

$$L(\theta) = 2R + 2d \cdot \sin\left(\frac{\theta}{2}\right) - 2(R-B) \cdot \cos\left(\frac{\theta}{2}\right),$$

TABLE 2 Design specifications of K-FLEX

Joint Configuration	(Overtube) Trans-Rot-Bend-Bend (Instrument) Trans-Rot-Bend-Bend-Grasp
Overall diameter, mm	17
Payload, g	300
Length of flexible part, mm	1000



FIGURE 3 A standard endoscope has problems when dealing with exerting a payload. The bending section has (A) constant curvature when free bending but has (B) deflection and (C) shape distortion with exerting force

$$L_a = L(-\theta), L_b = L(\theta),$$

$$\Delta L(\theta) = L_a + L_b - 4B = 4 \cdot (R-B) \cdot \left(1 - \cos\left(\frac{\theta}{2}\right)\right), \quad (1)$$

where L_a is the length of the actuation wire cable in the pulling direction and L_b is that in the releasing direction. This relationship is especially important for continuum manipulators with n stacked rolling joints as shown in Figure 4. If an external force F is applied to the distal end with both ends of the driving wire fixed, the continuum manipulator is distorted into a symmetric S shape.¹⁴ The energy level accumulated in the continuum can be calculated using Equation (1).

$$\Delta E_p = \int_{x_0}^{x_0 + \Delta L} T_{\text{wire}} \cdot dx = T_0 \Delta L + \frac{1}{2} k \Delta L^2, \quad (2)$$

where T_0 is an initial tension applied to the tendon and k is the stiffness of each wire cable assuming as a spring. ΔL is an amount of change in length of the driving wire cable and can be calculated as

$$\begin{aligned} \Delta L &= \left(\sum_{i=1}^n \Delta L_a(\theta_i) \right) + \left(\sum_{i=1}^n \Delta L_b(\theta_i) \right) + 2 \left(\sum_{i=1}^n \Delta L_c(\theta_i) \right) \\ &= 4 \cdot (2R-B) \sum_{i=1}^n \left(1 - \cos\frac{\theta_i}{2} \right), \end{aligned} \quad (3)$$

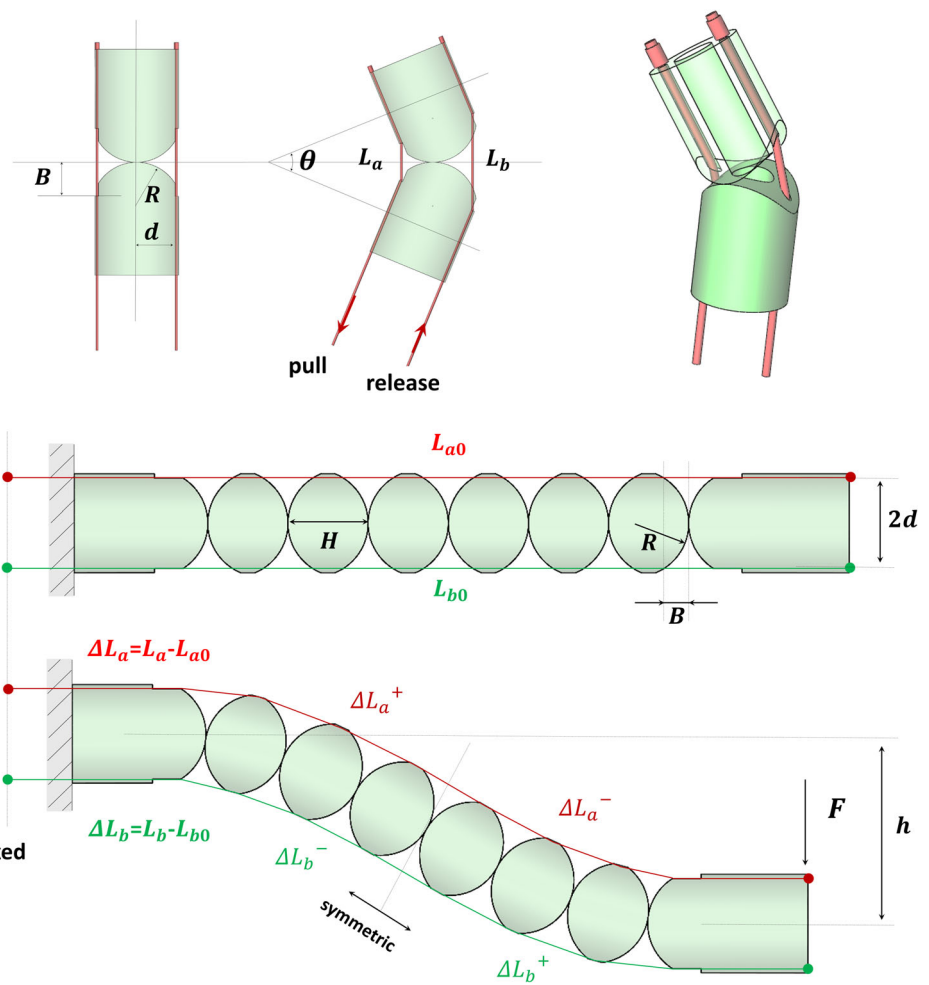
which includes the change in length of four wire cables. The subscript of ΔL_c indicates the constraining wires that pass through the top of the rolling surface. They are used not only to prevent torsional slippage of the rolling but also to actuate the other direction of bending. To estimate the deflection h against the external force F , the virtual work principle could be applied, which implies that the amount of accumulated energy equals to the work done by the external force.

Substituting Equation (3) to (2), we obtain

$$\begin{aligned} \int_0^h F dx &= \Delta E_p = 4T_0(2R-B) \cdot \sum_{i=1}^n \left(1 - \cos\frac{\theta_i}{2} \right) + 8k(2R-B)^2 \\ &\quad \cdot \left(\sum_{i=1}^n \left(1 - \cos\frac{\theta_i}{2} \right) \right)^2, \end{aligned}$$



FIGURE 4 The operating principle and variable definition of a rolling joint. The continuum manipulator is distorted into an S-shape when an external force is applied



$$F = 4T_0(2R-B) \cdot \frac{d}{dh} \sum_{i=1}^n \left(1 - \cos \frac{\theta_i}{2}\right) + 8k(2R-B)^2 \cdot \frac{d}{dh} \left(\sum_{i=1}^n \left(1 - \cos \frac{\theta_i}{2}\right)^2\right), \quad (4)$$

where $\sum(1 - \cos(\theta_i/2))$ is a function of h and H . This term should be minimized since each joint angle will be configured toward minimizing the accumulated energy. Rewriting in mathematical equation,

$$\operatorname{argmin}_{\theta_i} \sum_{i=1}^n \left(1 - \cos \frac{\theta_i}{2}\right) \text{ such that } \sum_{i=1}^n \sin \left(\sum_{k=1}^i \theta_k\right) = \frac{h}{H}. \quad (5)$$

The constraint was derived from the condition that the sum of the projections of the height of each link in the vertical direction equals the deflection h . Given the number of links n , this optimization problem can be solved by simplifying the nonlinear term as the polynomials assuming that $\theta \rightarrow 0$.

It is noteworthy from Equation (4) that the resistance increases as the difference between $2R$ and B increases. In other words, it is advantageous to design the difference $2R - B$ larger to make a continuum manipulator robust against an external force. In order to design a robust continuum manipulator, this study selected the design parameters on the basis of the following guidelines and considerations.

1. Working range of bending

$$2n \cdot \sin^{-1} \left(\frac{d}{R} \right) \geq \theta_{\text{req,max}}.$$

2. Minimum length of the moment arm

$$d \cos \left(\frac{\theta_{\max}}{2n} \right) \pm (R-B) \sin \left(\frac{\theta_{\max}}{2n} \right) \geq D_{\text{req,min}}.$$

3. Radius of curvature

$$H \cdot \frac{n}{\theta_{\max}} \leq \rho_{\text{req,min}} \quad (H = \text{link length}).$$

4. Select R and B maximizing S

$$\text{Resistance against distortion } S = 2R - B.$$

These main criteria can be calculated from the geometry between the rolling links. In this study, these requirements were defined with reference from our experience and the characteristics of standard

endoscopes as $\theta_{req, max} = 100^\circ$, $D_{req, min} = 5$ mm, and $\rho_{req, min} = 40$ mm. The required minimum length of the moment arm was calculated from the payload capability of 300 g. The final variables R and B used for the initial prototype were selected to maximize $2R - B$ within a feasible range of the above constraints as $R = 13$ and $B = 1.3$.

2.3 | Workspace analysis and mapping strategy

Many platforms employ commercial master devices to control their surgical robots. In spite of their ease of accessibility and compact design, there exists a risk of losing intuitiveness due to the different kinematic structures to the slave robot, which results in degrading the performance of surgical tasks. The commercial master device is not suitable for mapping to the proposed robot as the redundant 2 DoFs may cause confusion to the operator.

In this study, we have developed a master manipulator with a kinematic structure similar to that of the surgical instrument and the overtube (Figure 5). The common insertion movement was directly mapped and scaled with the translation of the master device. A gimbal mechanism was constructed on a translational base creating three independent orientational motions. The three axes of the yaw-pitch-roll joint intersect at one point where the operator can place the forearm. The biasing weight around the pitch axis was compensated by a spring-based mechanism.

Figure 6 shows an integrated kinematic drawing of the K-FLEX system. Coordinates were set up and attached to each of the joints based on the Denavit-Hartenberg (D-H) convention. On the basis of the forward kinematics equation, the reachable workspace of the robot was obtained as shown in Figure 7. Both overtube and surgical arm create a cylindrical workspace by their joint configurations of translational, rolling, and bending movement. The overtube has a larger workspace with a cross-sectional diameter of 150 mm so that it could expand the local workspace created by the surgical arm. Each of the surgical arms creates a smaller but delicate workspace with a cross-sectional diameter of 41 mm. The bimanual arm has an intersectional area of which the cross-section can be approximated as an ellipsoid with two principal axes of 38 mm (vertical) and 30 mm (horizontal). The translational motion ranges within 190 mm for the overtube and 53 mm for the surgical arm so that the cross-sectional area can be expanded along the main stem. As shown in Figure 7A, it

was confirmed that the global workspace sufficiently contains the peg transfer task area of the Fundamentals of Laparoscopic Surgery (FLS), as well as the working range of cholecystectomy.¹⁵ It could be presumed that the obtained area covers the endoluminal procedure since it also contains the working range of the standard endoscope.

A mapping strategy between the master device and the slave robot should be implemented in such a way that the overtube and two surgical arms are controlled by a pair of master devices. The master devices are assigned to each of the two surgical tools, and the left master device is switched to operate the overtube by a foot clutch when the workspace of the surgical tool requires expansion. The overtube could be intuitively manipulated by the master device since it has the same joint arrangement as the surgical instrument. The mathematical expression to match the orientation of the end effector with the orientation of the grasping tip of the master device is as follows.

$${}^b_3 T_{\text{master}} = {}^e_8 T_{\text{inst}},$$

$$\begin{bmatrix} \dots & n_{12} & \dots \\ \dots & n_{22} & \dots \\ n_{31} & n_{32} & n_{33} \end{bmatrix} = \begin{bmatrix} \dots & c_{p2}s_{r2} & \dots \\ \dots & c_{r2}c_{p2} & \dots \\ -c_{p2}s_{y2} & s_{p2} & c_{p2}c_{y2} \end{bmatrix},$$

$$\begin{bmatrix} d_2 \\ \theta_{r2} \\ \theta_{p2} \\ \theta_{y2} \end{bmatrix} = \begin{bmatrix} d_e + m_1 \cdot \lambda_2 \\ \tan^{-1}(n_{12}/n_{22}) \\ \tan^{-1}\left(n_{32}/\sqrt{n_{12}^2 + n_{22}^2}\right) \\ \tan^{-1}(-n_{31}/n_{33}) \end{bmatrix}. \quad (6)$$

Because it has the same joint configurations with the surgical instrument, the overtube can be mapped into the master device using the same equation as above (${}^b_3 T_{\text{master}} = {}^b_3 T_{\text{overt}}$). As a result, all joint angles of the surgical arm and the overtube can be obtained from the master device containing the operator's motion information. a_t and d_t are the distance of triangulation, which were set to zero for further miniaturization in this study. λ_1 and λ_2 are the scaling factors of translational motion.

Finally, the inverse kinematics results were put into a kinematic simulator, which facilitates the validation of kinematic equations and intuitive interpretations prior to operating the robot system. It visualized the robot's motion at a cycle of 20 milliseconds. The mapping

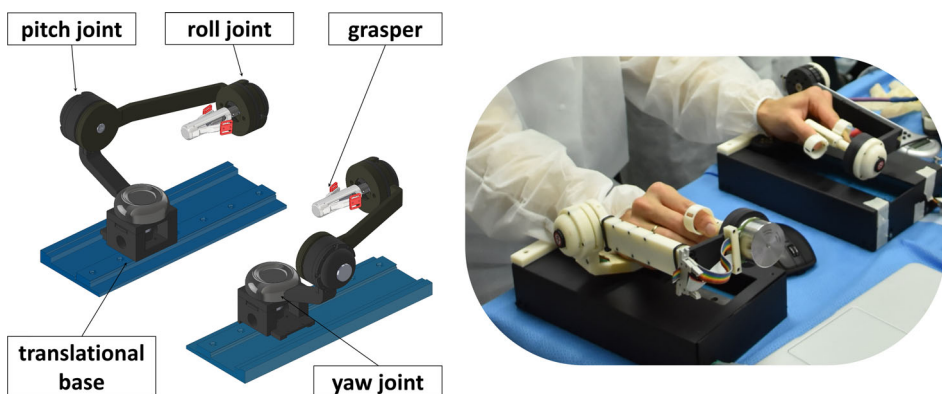
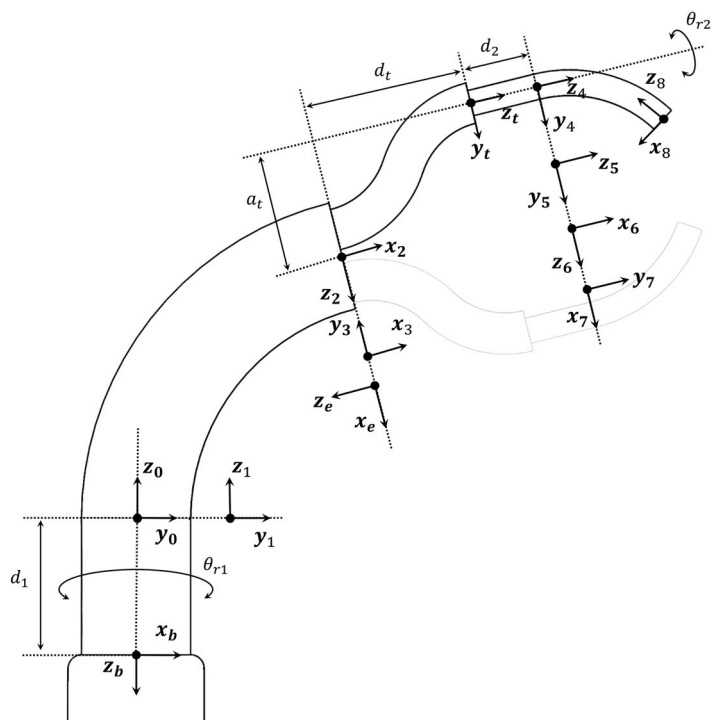
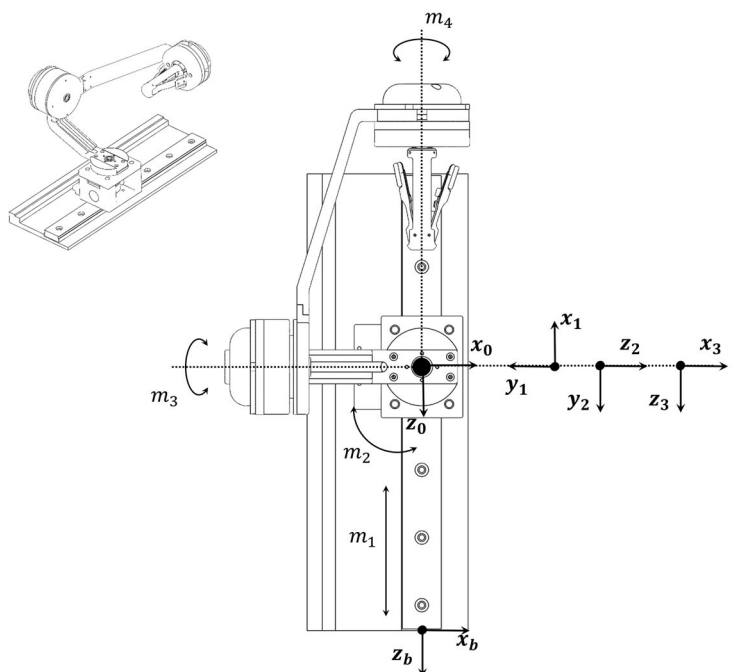


FIGURE 5 The master device has been developed with a similar kinematic structure to the surgical instrument



i	α_{i-1}	a_{i-1}	d_i	θ_i
0	180°	0	$-d_1$	-90°
1	0	0	0	θ_{r1}
2	-90°	-	-	$-90^\circ + \theta_{p1}$
3	-90°	-	-	$\theta_{y1}-90^\circ$
e	90°	0	0	0
t	180°	$\pm a_t$	$-d_t$	-90°
4	0	0	d_2	0
5	0	0	0	θ_{r2}
6	-90°	-	-	$-90^\circ + \theta_{p2}$
7	-90°	-	-	$\theta_{y2}-90^\circ$
8	90°	0	0	0



i	α_{i-1}	a_{i-1}	d_i	θ_i
0	0	0	$-m_1$	0
1	-90°	0	0	$90^\circ + m_2$
2	90°	0	0	$m_3 + 90^\circ$
3	-90°	0	0	$m_4 - 90^\circ$

FIGURE 6 Integrated kinematic drawing of the K-FLEX system. Coordinates were set up and attached to each of the joints on the basis of the Denavit-Hartenberg (D-H) convention

strategy, inverse kinematics, and user preference have also been verified through the kinematic simulator.

2.4 | System implementation

Each component of the K-FLEX system has been implemented having the overall diameter of 17 mm including the overtube, two surgical

instruments with a diameter of 3.7 mm for each, and an endoscopic camera with high-definition quality (Figure 8).

In addition to strong overtube for satisfactory tissue manipulation, it is even more important to design strong surgical instruments to be able to hold the tissue firmly. The dimensional constraint of the surgical instrument is stricter, whose diameter should be less than 3.7 mm, sufficient for it to be inserted through the inner channel. To satisfy the requirement, we have made instruments modular to equip

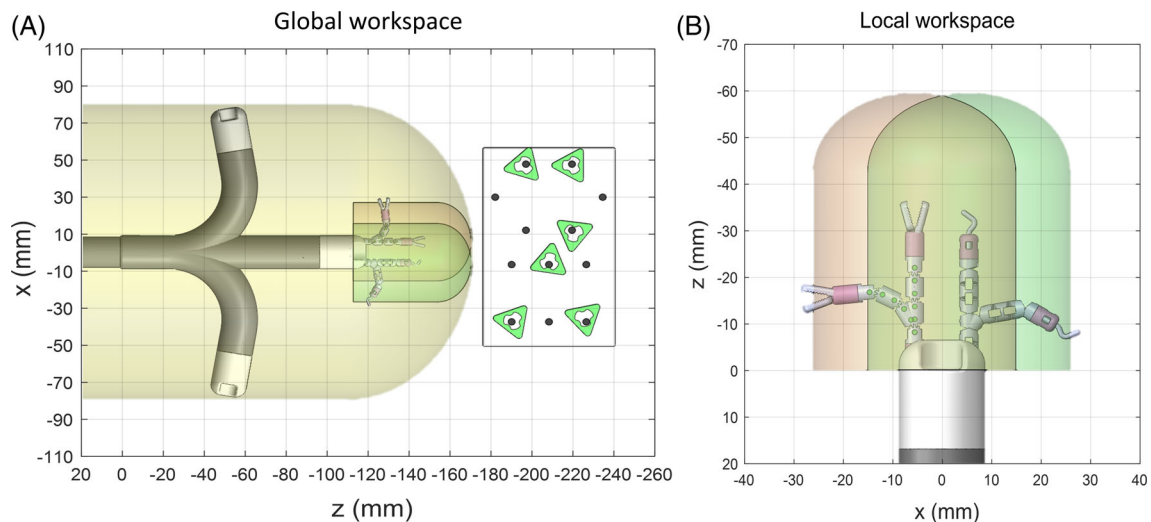


FIGURE 7 Workspace analysis of the proposed robot: (A) global workspace created by overtube and (B) local workspace by surgical arm

with various joint mechanisms for each purpose. The rolling continuum joint proposed in this study was customized for monopolar cautery and forceps, having different variables with the overtube ($R = 1.5$ mm, $B = 1.2$ mm). Since the proposed mechanism in this study was not able to meet the maximum payload requirement in 3.7 mm diameter, we adopted a special joint mechanism, which is called a constrained continuum (CC), to create a large amount of lifting force. The CC mechanism constrains the redundancy of continuum mechanically using auxiliary links to create a larger payload, which resulted in handling a maximum payload of 300 g with a diameter of 3.7 mm.¹⁶ Because the CC joint is limited in one bending motion, it was applied to the surgical instrument of traction to manipulate large organs, while the proposed rolling joint in this study was utilized to the suturing and cauterizing tools with more dexterous operations of two-directional bending.

The proposed manipulator is composed of a series of lumped links, actuation wire cable, and its sheath. The lumped links were 3D-printed with acrylonitrile butadiene styrene (ABS), which is a common thermoplastic polymer with an elastic modulus of 2200 MPa. The 7 × 7 stranded wire cables with the outer diameter of 0.54 mm were used for the actuation. The wire cables and sheath was manufactured with stainless steel (SUS 304), which is widely used for medical devices.

Elongation of the driving wire cable greatly affects the payload characteristics of the manipulator. A tensile strength test was conducted to figure out the stiffness of the driving wire cable. A motor and a load cell were set up and attached to the end of the wire cable while the other end was fixed to a base. Considering the sheath covering a wire cable is also deformable by a compressive force according to the cable elongation, we used a bundle of sheath and wire cable as one specimen. The tensile force was linearly applied between 0 and 40 N, while the amount of actuation length and the tensile force were measured simultaneously. As a result of eight specimens with a length of 1000 mm, the stiffness of tendon-sheath bundle was measured as 7.9 ± 1.0 N/mm on average with standard deviation. The deformation

of the lumped links was presumed to be negligible compared with the tendon-sheath bundle.

The integrated robot has a total of 14 DoFs including two surgical instruments and an overtube. All movements of the robot are controlled at a cycle of 1 millisecond based on the Linux operating system. In each cycle, 10 DoFs of the user's motion information are input into Equation (6) to obtain 14 joint angles of the robot based on the mapping strategy. Then, each joint angle is substituted to an amount of driving length of an antagonistic wire cable using Equation (1) and finally converted into the motor joint angle. A kinematics graphics model of the robot was displayed on a part of the screen to feedback the robot's configuration to the user.

2.5 | Payload experiment of the proposed manipulator

To verify the payload capability of the proposed manipulator, the first experiment was designed to identify how significantly the design parameters affect the stiffness of the manipulator. The proposed continuum was prototyped to have various design parameters ($R = 5, 10, 15$, and 20 mm), and a bending section of the standard endoscope was prepared for comparison. The other variables were purposefully set to be the same as those of the standard endoscope including the outer diameter and length of the continuum ($B = 1.3$ mm, $D_{\text{outer}} = 13$ mm, $L_{\text{bend}} = 83$ mm, $n = 7$, $T_0 = 30$ N, and $k_{\text{act}} = 7.9$ N/mm). Given the parameters, we solved the optimization problem from Equation (5) and obtained the final equation as follows.

$$F = \frac{T_0(2R-B)}{27} \frac{h}{H^2} + \frac{2k(2R-B)^2 h^3}{54^2} \frac{h^3}{H^4}$$

The base part of the continuum was firmly fixed using a customized jig while a 3D tracking sensor was attached to the point where the distal end of the surgical tool will be located. As a measuring

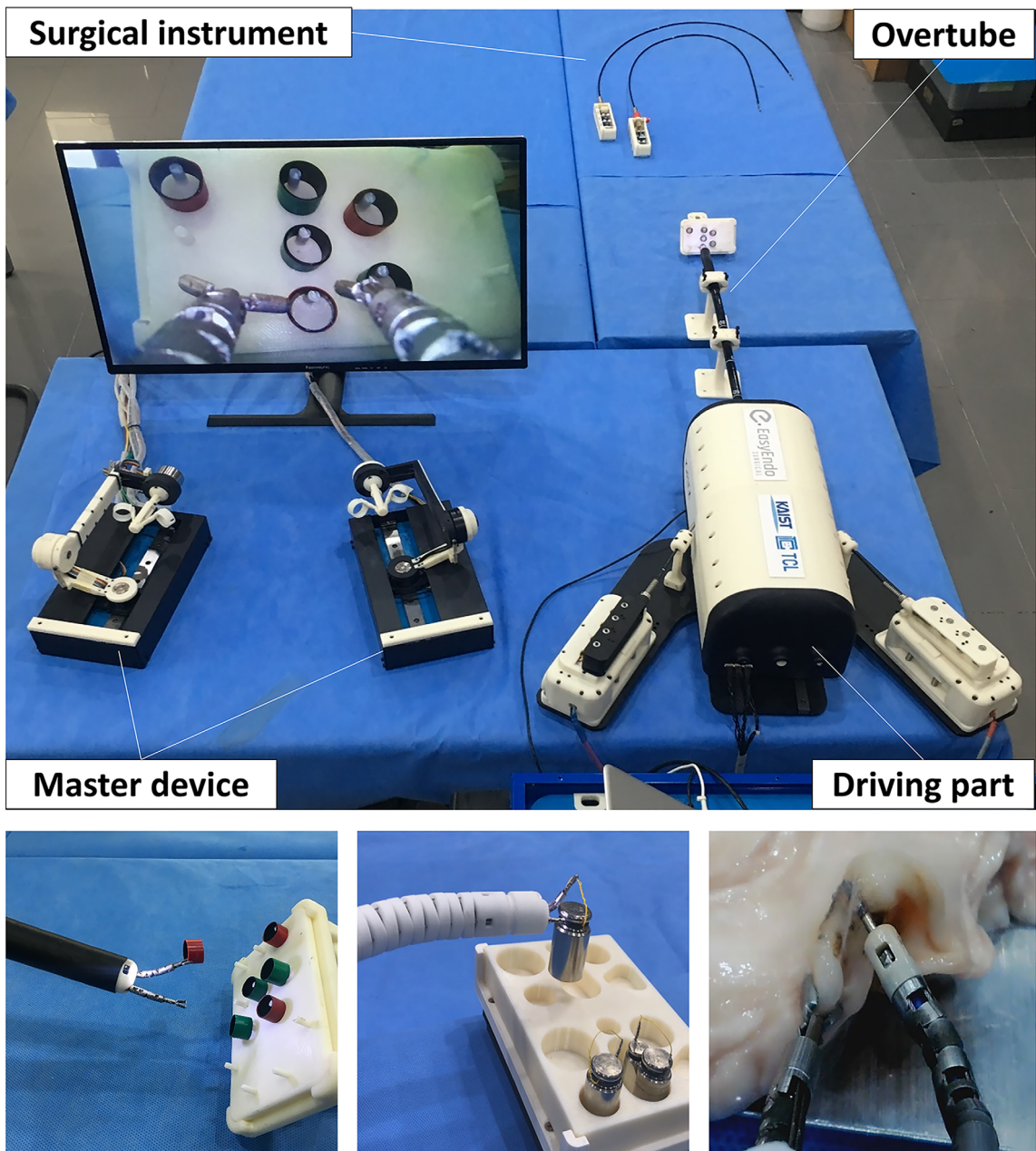


FIGURE 8 The K-FLEX system has been implemented having an overall diameter of 17 mm including the overtube, two surgical instruments, and an endoscopic camera. Three kinds of benchtop tests were performed to verify the feasibility of the proposed system

device, a commercial product, Aurora, from Northern Digital Inc, was chosen, which is an electromagnetic tracking system delivering 0.88 mm in positional accuracy. The flexible part was 1000 mm long, and a tendon-sheath mechanism was used to ensure flexibility. The manipulator was straightened, and each weight in a range of 50 to 300 g was hanged at the distal end. Then, the deflection of the end tip was recorded while increasing the weight in 50-g intervals. Finally, the stiffness for each R was calculated from the measured data.

The second experiment aimed to verify the payload handling performance of the prototype, on the basis of the final selected design variables. This could be verified by measuring the trajectory variation while the manipulator is actively bending under various payloads. With the

same experimental setup, the position of the end tip was recorded in real-time, while the manipulator was commanded to move through its full working range of -90° to 90° three times. The procedure was repeated with various weights of 0, 100, 200, and 300 g. Finally, an amount of variation was calculated between the trajectories.

2.6 | Benchtop tests of the integrated system

To verify the feasibility of the integrated system, three kinds of benchtop test were performed, which features basic surgical tasks. The benchtop tests were designed to demand the reachable workspace,



accuracy, and maneuverability, which is required in surgical operation. The first was a ring transfer test, which is a representative skill-assessment tool of FLS. The testbed was designed to have the same dimensions as FLS but with smaller transfer rings, as the grasper of the surgical instrument is more miniaturized. Following the instructions of FLS, the task is completed by moving six rings from the left side to the right side of the pegboard and then reversing the process.

The second benchtop test was devised to verify the traction and manipulation capability of heavy weights such as the liver, stomach, and bowel. In the second task, the operator was asked to control the robot remotely to perform the pick-and-place task, which is picking the weight up from the left side and placing it into the correct fitting hole on the right side.

Finally, an ex vivo test was conducted to verify the capability of manipulation and dissection using real tissue as the prior step to in vivo animal trials. The task was intended to perform a part of the endoscopic submucosal dissection (ESD), which is a standard endoluminal technique but considered technically difficult and challenging using a conventional flexible endoscope. An ex vivo stomach of a pig was prepared cleanly on a grounding pad. Circumferential marking with a 30-mm circular shape and submucosal injection were completed beforehand. Then, the operator, who is an expert endoscopist, was asked to control master device to complete the task using the proposed robot. The completion of the task was defined as precutting the mucosa along the circumferential marking and completely dissecting the submucosa. The left arm of the robot was outfitted with a grasping end effector, while the right arm utilized monopolar cautery.

3 | RESULTS

3.1 | Payload performance verification of the proposed manipulator

Figure 9 shows the result of a stiffness comparison for design variables. In all cases, the deflection linearly increases following the

increasing external force. The maximum deflection occurred at the 3-N payload within range of 18 to 45 mm. The deflection under the same payload was significantly decreased as the rolling radius R increases ($h = 45$ mm in $R = 5$ mm vs $h = 18$ mm in $R = 20$ mm). The difference in the amount of deflection, however, declined at the higher R as shown by the smaller changes in curves between $R = 15$ and 20. In contrast to the proposed manipulator, it was difficult to predict the motion of the standard endoscope since it showed an arbitrary increase in deflection. It was observed during the experiment that the end tip was outside the measurable area when weighed over 2 N, so we could not record the data in this range. The end tip was pointing down about 40° , and it seemed that it could not sustain any more weight.

Figure 10 shows the trajectory of the developed manipulator under various payloads. The simulated trajectory was marked with a dotted line, which was calculated from the forward kinematic equations. The enlarged figure clearly shows the differences between the trajectories. It should be noted that the no-load trajectory forms a shape of a thin crescent with a maximum width of 4.7 mm. We could infer that this is because, depending on the moving direction of the manipulator, the friction between the links and wire cables causes a difference in tension propagation of the antagonistic wires, resulting in a difference in rolling angle distribution. However, the no-load trajectory moving upward is almost identical to the simulated trajectory, having a maximum variation of 1.4 mm.

On the whole, each of the trajectories was found to be asymmetric between the upper and lower bending. The trajectories move to the direction of gravity as the payload becomes larger. Besides, even though the trajectories had the same input command, they present different turning points also moving downward along the trajectory due to the deflection of the end tip. The maximum variation between the trajectories was measured as 7.5 mm, which occurred between the no-load and the 300-g weight. It is also worth noting that the position of the two turning points of the upper and lower bending are biased even in the no-load trajectory, which are positioned at 100° and -79° of a bending angle, respectively. This is because of the

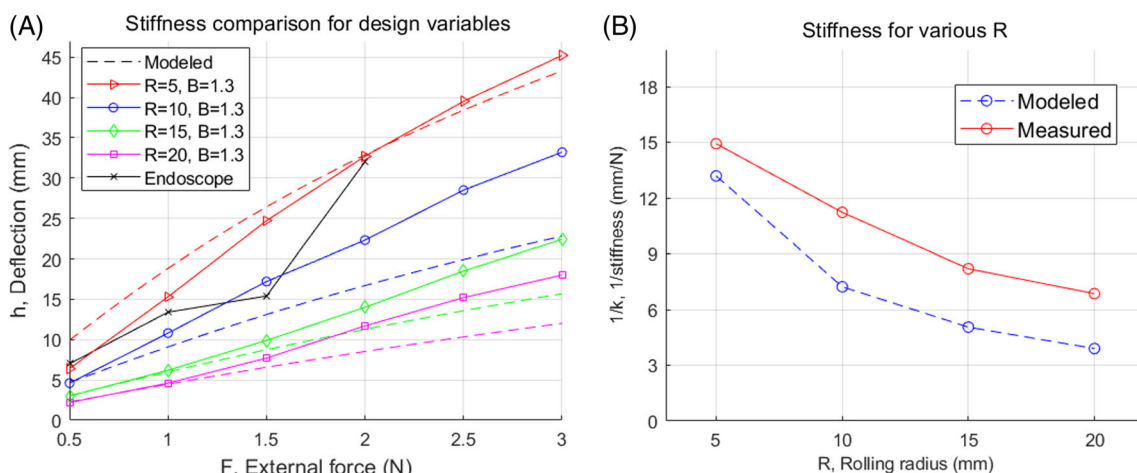


FIGURE 9 Stiffness comparison result for design variables. (A) Deflection linearly increases with external force, (B) Slope of the deflection curve decreases as R increases

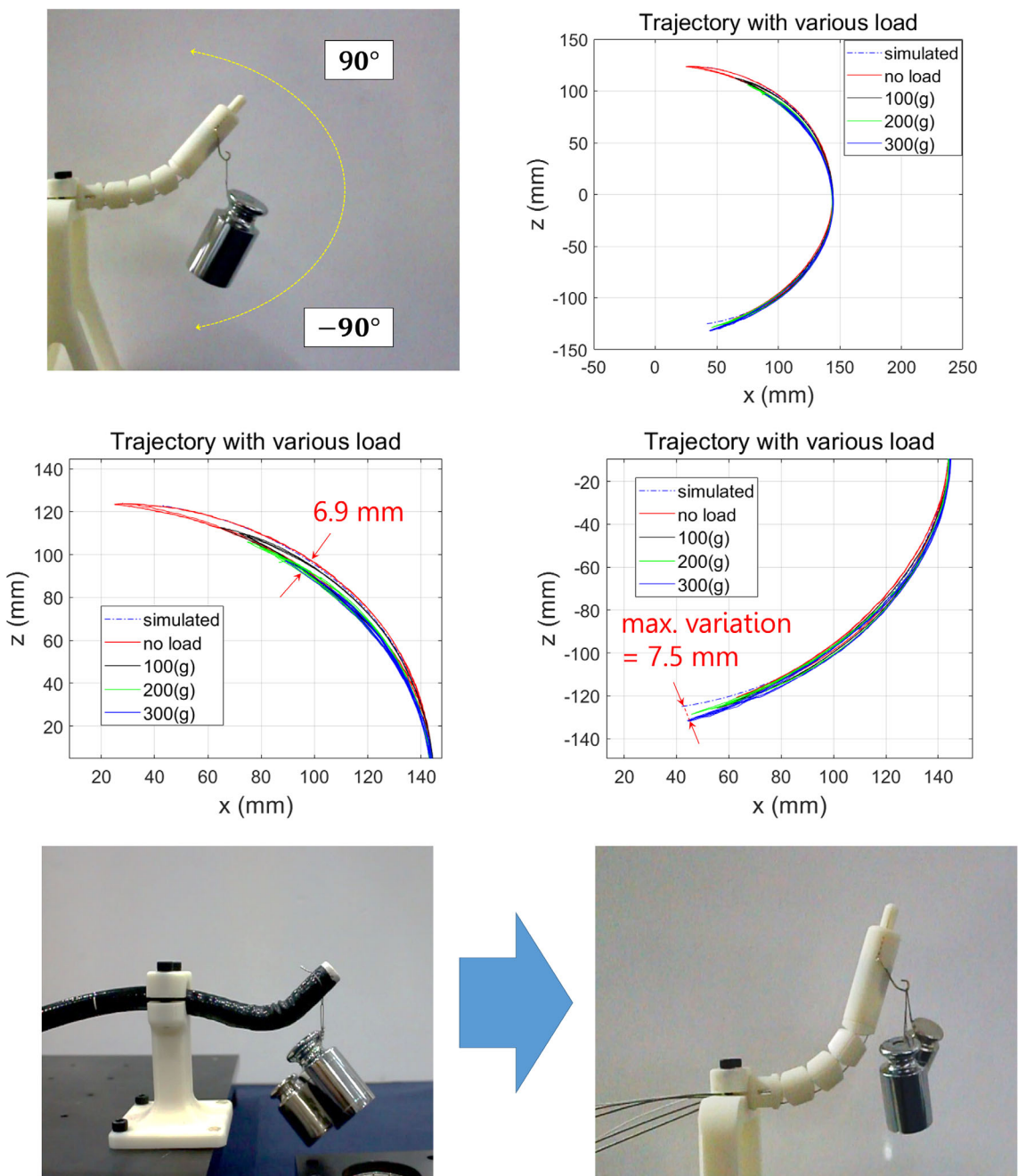


FIGURE 10 Trajectory variation under various payloads. The maximum variation between the trajectories was measured as 7.5 mm when dealing with a weight of 300 g

biased neutral (starting) posture of the manipulator. The bias with the amount of 10° occurred from the difficulties of calibrating the exact actuation position of the wire cable even when the manipulator is at the neutral position.

3.2 | Benchtop test results

A total of 12 repetitions of the peg transfer tasks were performed. For each trial, the completion time and drop occurrence of the ring

were measured. The result of average completion time was 203 ±35 seconds with two instances of drop occurrence in total. The drops happened because of the weak grasping caused by the inappropriate approaching angle of the tool tip. Unlike the existing laparoscopic platforms, the surgical tool tip was not able to make arbitrary orientation in 3D space because of the restriction of DoFs. Although it is difficult to assess the effectiveness of this result, as there is no clear criterion or comparative data of other flexible platforms, the obtained result was satisfactory considering the smaller size and workspace and the limited DoFs compared with that of the



laparoscopic platforms. We could show the possibility of tissue manipulation and accurate positioning of the proposed robot.

In the second task, the operator controlled the robot to grasp the string hanging each weight. During a total of five repetitions of the pick-and-place tasks, all the weights in a range of 10 to 100 g could be smoothly and successfully moved into the fitting hole. No circumstances of any structural failure, malfunction, or lack of workspace were encountered during the tasks. The payload handling capability of the integrated system could be confirmed.

As a result of the ex vivo task, it was observed that the tissue was grasped and pulled in various directions using the left surgical arm and then dissected using the right surgical arm with tension applied to the tissue. The average times of completion of the two procedures were 560.5 seconds for precutting and 603.0 seconds for dissection. The dissected area was measured as 924.5 mm², which is a slightly larger area than that of a circle 30 mm in diameter. Consequently, the dissection speed was calculated as 92.7 mm²/min. This outcome shows that the dissection using K-FLEX was almost two times faster compared with the result of a previous procedure that the same operator conducted using a standard endoscope (47.5 mm²/min).¹⁷ We observed that the difference mainly came from the traction and cutting motion in various directions, facilitated by the enhanced dexterity of the bimanual arm. It was confirmed that the desired lesion of the tissue could be successfully manipulated and dissected using the proposed robot.

4 | DISCUSSION

Although a continuum manipulator is essential in flexible platforms, it has inherent problems, which are the shape distortion and deflection during payload handling. To overcome these problems, we proposed a continuum manipulator in which the shape of the rolling link is designed so that the accumulated energy level is minimized when the continuum has a constant curvature. The continuum manipulator has been analyzed on the basis of energy minimization. In addition to the description of operating principles and analysis of the rolling joint, this paper also provides a variable selection guideline to design a robust continuum manipulator. Finally, the proposed manipulator has been applied to a flexible endoscopic surgery robot, K-FLEX, and the feasibility of the system has been verified using several preliminary tests. The main contribution of this study includes the design, analysis, and verification not only for a strong continuum manipulator but also for a flexible endoscopic surgery robot system.

One of the major outcomes of this study is the significant enhancement of the payload capability of the flexible manipulator. Unfortunately, it is very difficult to evaluate our results in comparison with those of existing platforms because there are rarely any quantitative payload/stiffness results revealed in the literature, in contrast to results regarding the overall diameter, which can easily be found. However, given the fact that most of the existing platforms have utilized the commercial endoscope based on the same mechanical bending structure rather than customizing it, we can presume that they

should have difficulties in handling the payload of 300 g as shown in Figure 3. It is noticeable from Figure 9A that the standard endoscope failed to support over 2 N of payload, while the proposed manipulator enhanced the payload capability up to 3 N with a relatively small amount of deflection.

It is noteworthy that MASTER⁵ and CYCLOPS⁹ have presented higher payload capabilities (3 N and 7.5 N, respectively) with their novel design of surgical arms. However, their overall dimensions have been highly increased consequently (22 mm and 18 × 30 mm, respectively), which are considered as insufficient miniaturization for gastric insertion. In addition, the two platforms are no exception to the use of the standard endoscope, which means that the stronger overtube is demanding to support their manipulating force.

The stiffness comparison verified that the proposed manipulator is superior to the standard endoscope in payload handling and that the design variable R considerably affects the stiffness of the manipulator. Even though the modeling was not satisfactory to predict the exact value of stiffness, we see that it tends to give predictions that are parallel to the experimental data from corresponding tests. Figure 9B shows that the slope of the deflection curve decreases as R increases, indicating that the correlation of the modeling seems to be consistent with the result of the measured data. On the whole, the slope of the measured curve was offset in the direction of increasing deflection. On the basis of our experience, one possible cause is that the small clearances in mechanical parts accumulate errors and result in the deflection offsets of the assembled manipulator. It was considered to be important to adjust the tolerance between the tendon-rolling links and the tendon-sheath pair. Friction in the routing of wire cables may also contribute to these errors.

The trajectory experiments in this study showed the maximum variation of the trajectory of 7.5 mm with a weight of 300 g. Since the accuracy requirements of the flexible manipulator have not been studied yet, the obtained result is hard to evaluate. Even though this result needs to be verified through further experiments to identify how effective the resultant value is in real surgery, the variation amount of 7.5 mm corresponds to 4% of the operating diameter of 240 mm. Fortunately, the image-guided teleoperation enables the operator to compensate these errors using visual feedback from the video image. As an example, the standard endoscope also has a considerable amount of inaccuracy, but it is compensated by further movement of the endoscopist until the desired view is achieved. In this study, the proposed system could achieve higher accuracy with visual feedback from the user. However, the operator's cognitive compensation may increase the physical and mental burden, which degrades the overall surgical performance. To further increase the accuracy of the manipulator, it is worth applying the visual servoing and antagonistic tendon control algorithm as further works.

The possibility of using K-FLEX has been verified through the simulated surgical tasks. Further improvements should precede *in vivo* experiments. Even though the diameter of the existing platforms varies within a range of 16 to 22 mm for gastric application,¹⁰ there are concerns from clinicians that the diameter exceeding 17 mm may not be enough for safe introduction for some Asians or for people having



a small natural orifice. Although no clear evidence or guidelines exist for the acceptable dimensions of such devices, we guess that a smaller diameter of the platform will facilitate more versatile applications in the gastrointestinal field and secure more working spaces. The down-sizing results in consequent problems, including loss of payload, DoFs, and reduction of other performance metrics. These trade-offs should be more researched and overcome.

Through the ex vivo experiment, we could assume that the approximate force required for traction and dissection of mucosa is estimated to be 50 to 100 g. The payload capability of the proposed manipulator was confirmed to be enough for the ex vivo task of this study. Since the demands on the platforms are very broad for each endoscopic procedure, further studies should focus on conducting more experiments using the proposed platform in various different procedures, and we hope to find possible applications in the gastrointestinal tract. Another observation during the ex vivo test was that the electronic components were affected by electrocautery equipment during the high intensity of cauterization. This phenomenon occurred even when the electronic devices had no direct contact with the electrocautery equipment. We finally solved this problem by insulating the mechanical parts from the cauterizing tool and by double-shielding the electric cables to reduce the influence from electromagnetic waves.

The developed surgical instruments were not as agile as laparoscopic surgical robots, and the users noted difficulties in object manipulation. For example, because of the deficiency of DoFs, it was difficult for the user to grasp the object with a more favorable approaching angle, which resulted in missing the object, discomfort in posture, and obstructing the view of the target. Flexible endoscopic platforms have commonly faced these problems as their spatial limitations are very strict. Studies on which DoF or joint combination is more important in endoscopic procedures may also play a significant role in this field. In spite of these dexterity limitations, the preliminary results have demonstrated the feasibility of the proposed flexible platform, which is significantly different from the standard endoscope.

In laparoscopic surgery, many technical requirements have been identified through several experiments of surgical tasks.¹⁵ Likewise, many efforts should be focused on investigating the requirements of each endoscopic procedure, which will accelerate the development of advanced endoscopic platforms. Finally, surgical performance using flexible robotic platforms will be much improved with advanced instruments specialized in certain subtasks, such as suturing devices, clip appliers, and traction tools.¹⁸ The development of a needle driver would be very useful for suturing tasks. Further works may also include a thorough user experiment, in vivo experiment, and quantitative results on mapping strategy.

The flexible platform is expected to overcome the limitations of rigid surgical robots. Since a flexible platform allows access to the target surgical site through a curved path, it has the potential to expand its application into other areas of surgery. The proposed continuum robot is versatile with its flexibility and enhanced payload capability and can also be applied to the gastrointestinal tract; ear, nose, and throat; and natural orifice transluminal endoscopic surgery (NOTES).

We believe that through flexible robotic technologies, surgeons will be able to conduct challenging procedures that have not yet been attempted.

ACKNOWLEDGEMENTS

This research was supported by Basic Science Research Program through the National Research Foundation of Korea (NRF) funded by the Ministry of Education (2008-0060621) and by the Global Center for Open Research with Enterprise Program through the Office of University-Industry Cooperation funded by the Korea Advanced Institute of Science and Technology. The authors are grateful to Joonhwan Kim, Jeongdo Ahn, Dongho Lee, Hansoul Kim, Donghoon Baek, Jaemin You, and Dr Seung Woo Lee for their support.

ORCID

Minho Hwang <https://orcid.org/0000-0002-9190-7876>

Dong-Soo Kwon <https://orcid.org/0000-0003-1540-3307>

REFERENCES

1. Fuchs K-H, Se BWJ. Transgastric small bowel resection with the new multitasking platform EndoSAMURAI™ for natural orifice transluminal endoscopic surgery. *Gastrointest Endosc*. 2012;76(8):2281-2287.
2. Thompson CC, Ryou M, Soper NJ, Hungess ES, Rothstein RI, Swanstrom LL. Evaluation of a manually driven, multitasking platform for complex endoluminal and natural orifice transluminal endoscopic surgery applications (with video). *Gastrointest Endosc*. 2009;70(1): 121-125.
3. Swanstrom LL, Kozarek R, Pasricha PJ, et al. Development of a new access device for transgastric surgery. *Gastrointest Endosc*. 2005;9(8): 1129-1137.
4. Léger A, Diana M, Halvax P, et al. Endoluminal surgical triangulation 2.0: a new flexible surgical robot. Preliminary pre-clinical results with colonic submucosal dissection. *The International Journal of Medical Robotics and Computer Assisted Surgery*. 2017;13(3):e1819.
5. Phee SJ, Low SC, Sun ZL, Ho KY, Huang WM, Thant ZM. Robotic system for no-scar gastrointestinal surgery. *Int J Med Robot*. 2008;4(1): 15-22.
6. Abbott DJ, Becke C, Rothstein RI, Peine WJ. Design of an endoluminal NOTES robotic system. Paper presented at: Intelligent Robots and Systems, 2007. IROS 2007. IEEE/RSJ International Conference on 2007.
7. Schuler PJ, Hoffmann TK, Veit JA, et al. Hybrid procedure for total laryngectomy with a flexible robot-assisted surgical system. *Int J Med Robot*. 2017;13(2):e1749.
8. Berthet-Rayne P, Gras G, Leibrandt K, et al. The i2Snake robotic platform for endoscopic surgery. *Ann Biomed Eng*. 2018;46(10):1663-1675.
9. Vrielink TJO, Zhao M, Darzi A, Mylonas GP. ESD CYCLOPS: a new robotic surgical system for GI surgery. Paper presented at: 2018 IEEE International Conference on Robotics and Automation (ICRA) 2018.
10. Yeung BPM, Gourlay T. A technical review of flexible endoscopic multitasking platforms. *Int J Surg*. 2012;10(7):345-354.
11. Arkenbout EA, Henselmans PW, Jelínek F, Breedveld P. A state of the art review and categorization of multi-branched instruments for NOTES and SILS. *Surg Endosc*. 2015;29(6):1281-1296.
12. Blanc L, Delchambre A, Lambert P. Flexible medical devices: review of controllable stiffness solutions. *Actuators*. 2017;6(3):23.
13. J-W S, K-Y K, J-W J, Lee J. Design considerations for a hyper-redundant pulleyless rolling joint with elastic fixtures. *IEEE/ASME Transactions on Mechatronics*. 2015;20(6):2841-2852.



14. Gravagne IA, Walker ID. On the kinematics of remotely-actuated continuum robots. Paper presented at: Robotics and Automation, 2000. Proceedings. ICRA'00. IEEE International Conference on 2000.
15. Lum MJ, Trimble D, Rosen J, et al. Multidisciplinary approach for developing a new minimally invasive surgical robotic system. Paper presented at: Biomedical Robotics and Biomechatronics, 2006. BioRob 2006. The First IEEE/RAS-EMBS International Conference on 2006.
16. Hwang M, Kwon D. Strong continuum manipulator for flexible endoscopic surgery. *IEEE/ASME Transactions on Mechatronics*. 2019;24(5): 2193-2203.
17. Hwang M, Lee SW, Park KC, Sul HJ, Kwon D-S. Evaluation of a robotic arm assisted endoscope to facilitate endoscopic submucosal dissection (with video). *Gastrointest Endosc*. 2019. <https://doi.org/10.1016/j.gie.2019.11.014>
18. Rattner DW, Hawes R, Schwartzberg S, Kochman M, Swanstrom L. The Second SAGES/ASGE White Paper on natural orifice transluminal endoscopic surgery: 5 years of progress. 2011;25(8):2441-2448.

SUPPORTING INFORMATION

Additional supporting information may be found online in the Supporting Information section at the end of this article.

How to cite this article: Hwang M, Kwon D-S. K-FLEX: A flexible robotic platform for scar-free endoscopic surgery. *Int J Med Robotics Comput Assist Surg*. 2020;16:e2078. <https://doi.org/10.1002/rcs.2078>